J Mater Sci (2010) 45:2002–2008
DOI 10.1007/s10853-009-4149-5

HTC2009

# Surface tension and density measurement of liquid Si–Cu binary alloys

**Masayoshi Adachi · Michael Schick · Juergen Brillo · Ivan Egry · Masahito Watanabe**

Received: 14 June 2009 / Accepted: 18 December 2009 / Published online: 5 January 2010


**Abstract** Surface segregation is very important for understanding the surface tension of binary systems. In case of a regular solution, the surface segregation is calculated using the Butler model. However, in the case of a complex system, like those forming intermetallic compounds, it is difficult to express the surface segregation. In order to discuss surface segregation in systems forming intermetallic compounds, we measured the density and surface tension of a Si–Cu binary system. We found the effect of clusters in both density and surface tension experimental data. The composition dependence of surface tension was expressed by a modified ideal solution model.

## Introduction

Because of their low density, aluminium-based alloys are widely employed for industrial use. The Al–Cu–Si alloys are particularly well suited for casting processes and hence are widely used. For accurate modelling of the casting process, thermophysical properties of the melt of alloys are required. In order to understand the Al–Cu–Si ternary system, it is important to know the thermophysical properties of each binary system. Today, the thermophysical properties of Al–Cu alloy and Al–Si alloy are available. In contrast, few thermophysical property data for the Si–Cu binary system have been reported. Therefore, the Si–Cu binary system is interesting from an industrial viewpoint.

The Si–Cu binary system is also interesting from the viewpoint of materials science. This system has a complex phase diagram in the region of Cu-rich composition. In particular, at a Cu-75 at.% composition, the solid phase contains intermetallic compounds [1].

The composition dependence of surface tension of binary alloys is estimated from the surface tension data of each pure component using the Butler model [2, 3]. Butler derived the surface tension of binary alloys assuming equilibrium between the bulk phase and the surface phase, which is regarded as a hypothetical independent phase. In this model, the difference between bulk and surface excess Gibbs energies is taken into account. However, when using regular solution expressions for the Gibbs energies, the effect of the existence of aggregates of intermetallic compounds is not taken into account. Recently, a model of surface tension of binary alloys with compound formation was proposed [4]. This model is an extension of the ideal solution model.

Therefore, in this research, we measured the density and surface tension of Si–Cu binary alloys to compare their bulk and surface properties. Density represents the bulk state while surface tension represents the surface state. From the results of these experiments, we compared our data with Butler model and the extension of the ideal solution model.

## Experiments

Si and Cu have a high melting temperature and high reactivity. Moreover, surface tension is strongly affected by sample contamination. Therefore, we used an electromagnetic levitation method to measure the density and

M. Adachi · M. Schick · J. Brillo · I. Egry
Institute of Materials Science in Space, German Aerospace Center, Linder Hoehe, 51170 Cologne, Germany

M. Adachi (✉) · M. Watanabe
Department of Physics, Gakushuin University, 1-5-1 Mejiro, Tokyo 171-8588, Japan
e-mail: 07241001@gakushuin.ac.jp

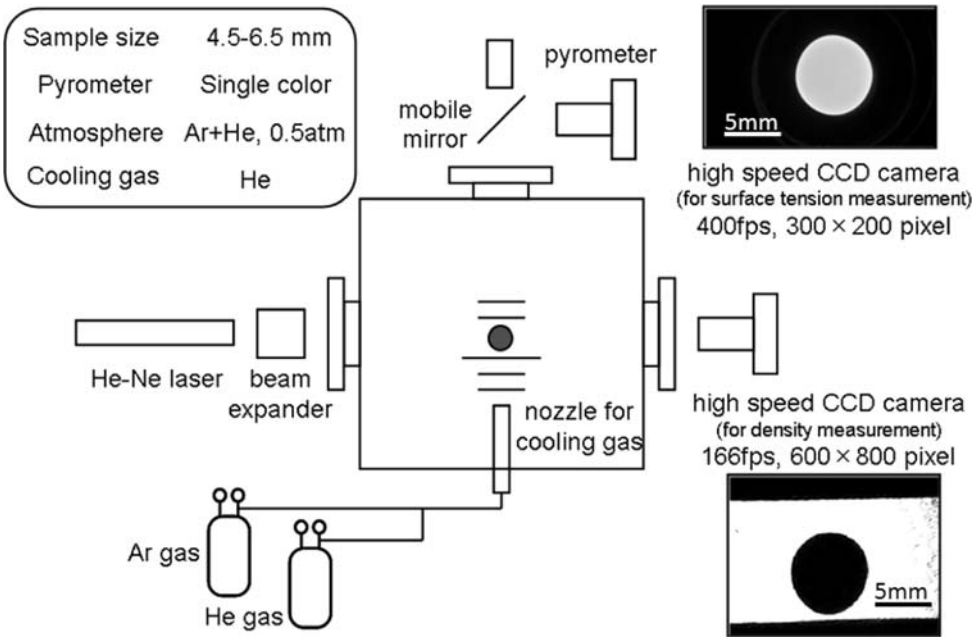


**Fig. 1** Schematic diagram of experimental apparatus for measuring density and surface tension of levitated droplet

surface tension to eliminate the effects of contamination due to chemical reaction with crucibles. The experimental facility is shown in Fig. 1. The vacuum chamber was evacuated to $10^{-4}$ Pa, and then filled with a 0.05 MPa Ar and He gas mixture. Temperature control is performed by exposing the droplet to a laminar flow of Ar or He gas from the bottom. The temperature of the sample was observed using a single colour pyrometer. Temperature data were adjusted by matching the observed melting to the known liquidus temperature.

The density of a levitated droplet can be measured from its shape, and its surface tension can be measured from frequencies of surface oscillation of the droplet.

## Evaluation of density

In order to eliminate the effect of deformation of the droplet along the vertical axis, the density of the droplet was evaluated using images taken from a horizontal direction. Moreover, to obtain the sharp edge of the droplet, we used a He–Ne laser light source for back illumination and recorded the droplet shadow image using a high-speed camera. In order to eliminate the light of non-parallel components, we used two lenses ($f = 80$ mm) and a pinhole ($\phi = 0.5$ mm). Details of measurement method are given in Ref. [5].

A levitated droplet performs surface oscillations due to electromagnetic force. Therefore, its equilibrium shape is determined by the average radius of multiple superimposed images using a common centre of mass. In this measurement, we obtained the averaged radius data from 1,500 images. The radius $r$ from the centre of mass of the droplet to the averaged edge was fitted by a series of Legendre polynomials of order six, as shown in the following equation:

$$r(\cos(\theta)) = \sum_{n=0}^{6} a_n P_n(\cos(\theta)). \quad (1)$$

The equilibrium droplet is assumed to have a rotationally symmetrical shape around the vertical axis. Therefore, volume of the droplet is calculated by

$$V = \frac{2\pi}{3} \int_{-1}^{1} r^3(\cos(\theta)) \mathrm{d}\cos(\theta). \quad (2)$$

The mass of the sample was measured before and after levitation to confirm the volume change from evaporation of the samples. For all of our measurements, this volume change is less than 0.5%. Finally, the density was calculated by dividing the mass by volume. Images of five calibration spheres of different sizes ($\phi = 4$–$7$ mm) were taken to calibrate in pixels the real volume of the droplet using Eq. 2. In this measurement, the scaling factor was between 0.016 and 0.017 mm/pixel.

## Evaluation of surface tension

Surface tension is obtained from the surface oscillation frequency of droplets [6]. Consecutive images taken from a vertical direction with a high speed camera yielded the oscillation frequencies. In order to observe the fundamental oscillation of the surface of the droplet, the high speed camera is operated at a frame rate of 400 Hz. As described later, all frequencies are obtained using fast Fourier transformation analysis of a few parameters of the radius of

the droplet. The resolution of the oscillation frequency spectrum depends on the number of droplet images. In this measurement, we obtained 4,096 droplet images for one measurement.

Surface tension is obtained from

$$\omega_R^2 = \frac{32\pi}{3}\frac{\gamma}{M}. \quad (3)$$

Here, $\omega_R$ is the fundamental oscillation frequency, $\gamma$ is the surface tension and $M$ is the droplet mass. For experiments under gravity, the surface oscillation frequency shifts and splits due to deformation of the levitated droplet. Therefore, we used a compensating formula [7]

$$\omega_R^2 = \overline{\Omega_2^2} - 1.9\omega_{tr}^2 - 0.3\omega_{tr}^{-2}\left(\frac{g}{R}\right)^2, \quad (4)$$

$$\overline{\Omega_2^2} = \left(\omega_{2,0}^2 + 2\omega_{2,\pm1}^2 + 2\omega_{2,\pm2}^2\right)\Big/5. \quad (5)$$

Here, $\omega_{tr}$ is the mean translational frequency of the centre of mass of the droplet. Details of the measurement method are given in Ref. [6].

In order to identify frequencies $\omega_{2,0}$, $\omega_{2,\pm1}$ and $\omega_{2,\pm2}$, the time dependence of $R+$ and $R-$ are extracted from the consecutive images. Here, $R+$ and $R-$ are the sum and difference of the radius along the $x$ axis ($Rx$) and $y$ axis ($Ry$), respectively, of the image of the droplet, with origin at the centre of mass of the droplet. The $m = 0$ mode has a peak only in the $R+$ spectrum, the $m = \pm1$ mode has a peak both in the $R+$ and $R-$ spectra, and the $m = \pm2$ mode has a peak only in the $R-$ spectrum. Therefore, it is possible to determine the frequencies of each mode. Moreover, the time dependence of the centre of mass and projected area of the droplet are extracted to obtain the translational frequencies of the centre of mass in three directions.

## Results and discussion

### Density

Figure 2 shows the temperature dependence of the density of Cu–Si binary alloys. The data of pure copper was taken from Ref. [5]. For all compositions of the samples, the density is a linear function of temperature. The values of standard deviation for each composition are less than 0.01 g/cm$^3$. Table 1 shows the temperature coefficient and density value at the liquidus temperature. Moreover, Fig. 3 shows the composition dependence of the density at 1370 K. The densities of pure copper and pure silicon are taken from Refs. [5, 8], respectively (for pure silicon, the value was extrapolated to 1370 K). It can be seen that the density is approximately a linear function of composition.

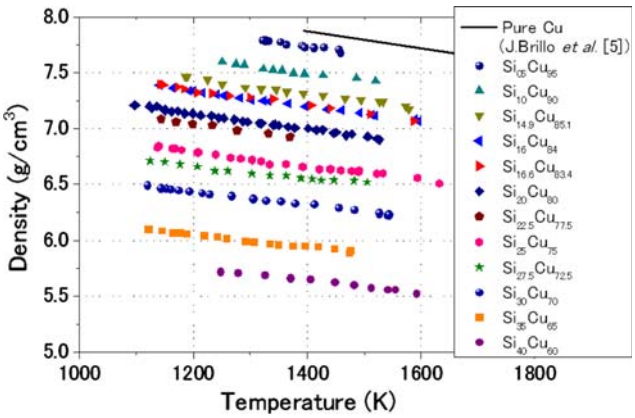


**Fig. 2** Temperature dependence of density of Si–Cu binary alloys. The *upper solid line* shows the density of pure copper reported by [5]

**Table 1** Temperature coefficient of density and density value at liquidus temperature for Si–Cu binary alloys

| | Liquidus temperature, K | Temperature coefficient, $10^{-4}$g/cm$^3$ K | Density at liquidus temperature, g/cm$^3$ |
|---|---|---|---|
| $Si_{05}Cu_{95}$ | 1311 | −7.012 | 7.794 |
| $Si_{10}Cu_{90}$ | 1246 | −6.308 | 7.591 |
| $Si_{14.9}Cu_{85.1}$ | 1159 | −6.728 | 7.471 |
| $Si_{16}Cu_{84}$ | 1125 | −6.725 | 7.383 |
| $Si_{16.6}Cu_{85.4}$ | 1118 | −7.042 | 7.403 |
| $Si_{20}Cu_{80}$ | 1094 | −6.951 | 7.206 |
| $Si_{22.5}Cu_{77.5}$ | 1131 | −6.805 | 7.088 |
| $Si_{24}Cu_{76}$ | 1132 | −5.729 | 6.796 |
| $Si_{25}Cu_{75}$ | 1131 | −6.274 | 6.831 |
| $Si_{27.5}Cu_{72.5}$ | 1114 | −5.144 | 6.703 |
| $Si_{30}Cu_{70}$ | 1075 | −5.921 | 6.505 |
| $Si_{35}Cu_{65}$ | 1164 | −5.503 | 6.071 |
| $Si_{40}Cu_{60}$ | 1235 | −5.668 | 5.737 |

In order to discuss the composition dependence, we calculated the molar volume of these samples at 1370 K. Figure 4 shows the molar volume of Si–Cu binary alloys. The solid line in Fig. 4 shows the volume calculated by the ideal solution model. The molar volume of the ideal solution is given by

$$V_{ideal} = C_{Si}\frac{m_{Si}}{\rho_{Si}} + C_{Cu}\frac{m_{Cu}}{\rho_{Cu}}, \quad (6)$$

where, $C_{si}$ and $C_{Cu}$ are the atomic concentrations, and $m_{Si}$ and $m_{Cu}$ are the molar masses of silicon and copper, respectively. Figure 4 shows that the difference between real molar volume and molar volume given from the ideal solution model exhibits composition dependence. This difference is called excess volume, which is expressed by

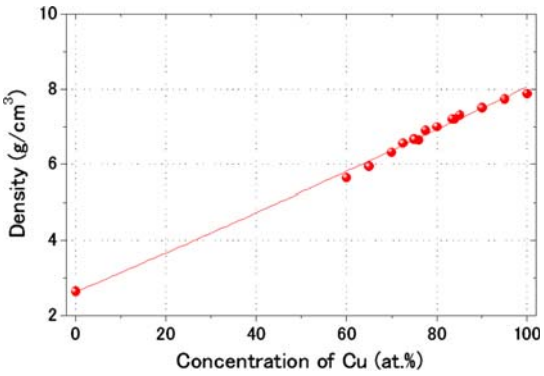


**Fig. 3** Composition dependence of density of Si–Cu binary system at 1370 K

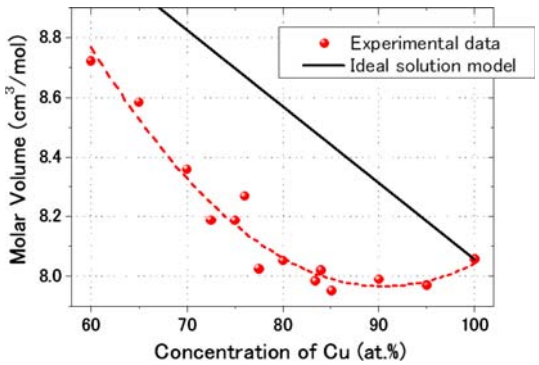


**Fig. 4** Composition dependence of molar volume of Si–Cu binary system at 1370 K

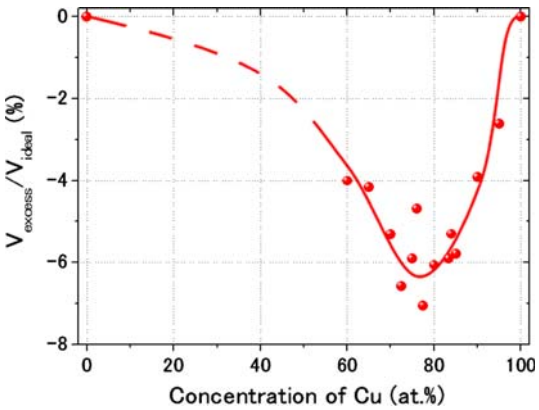


**Fig. 5** Composition dependence of excess volume divided by molar volume given by the ideal solution model. A minimum exists at Cu-75 at.%, which is the composition of the $\eta$ intermetallic phase

$$V_{\mathrm{E}} = V - V_{\mathrm{ideal}} = V - \left( C_{\mathrm{Si}} \frac{m_{\mathrm{Si}}}{\rho_{\mathrm{Si}}} + C_{\mathrm{Cu}} \frac{m_{\mathrm{Cu}}}{\rho_{\mathrm{Cu}}} \right). \quad (7)$$

Figure 5 shows the composition dependence of $V_{\mathrm{E}}/V_{\mathrm{ideal}}$. An extremum can be seen to exist around Cu75-at.%. Thus, the effect of atomic correlation becomes strong in this region. This composition corresponds to the intermetallic composition of the $\eta$ phase. This result, therefore, suggests that tiny aggregates of $Cu_3Si$ exist as metastable fluctuations in the liquid state of Cu-75at.%.

## Surface tension

Figure 6 shows the temperature dependence of the surface tension of Si–Cu binary alloys. For all compositions of the samples, the surface tension is a linear function of temperature in this temperature region. The standard deviations of each composition are less than 0.012 N/m. From this result of temperature dependence of surface tension, we obtained the composition dependence of the surface tension of the Si–Cu system at 1370 K. Figure 7 shows the composition dependence of surface tension and also the results obtained by Khilya G. P. et al. using the sessile drop method [9]. Their data shows qualitatively the same trend as ours, although they are somewhat lower quantitatively. This may be due to the higher environmental purity in levitation experiments. Table 2 shows the temperature coefficient and

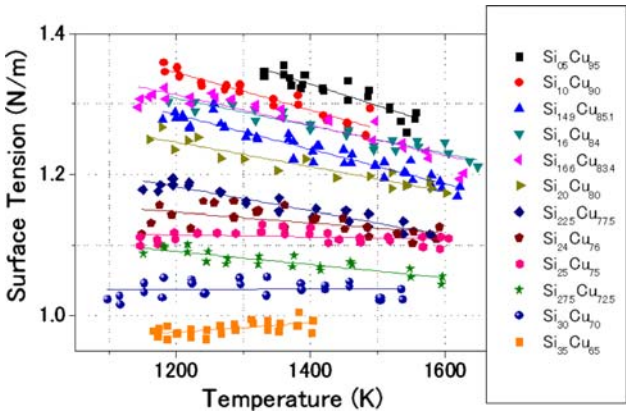


**Fig. 6** Temperature dependence of surface tension of Si–Cu binary alloys. In this temperature region, the surface tension shows a linear dependence on temperature

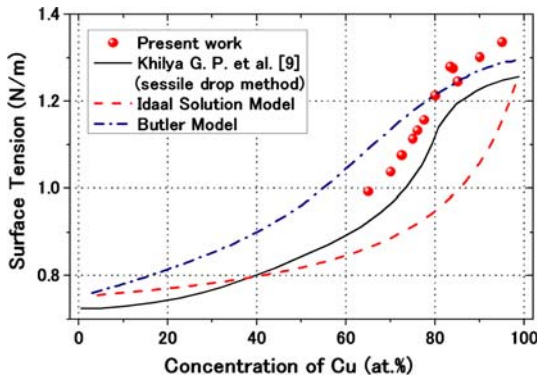


**Fig. 7** Experimental data and calculation results using the ideal solution model and the Butler model for the composition dependence of surface tension of Si–Cu binary system at 1370 K

**Table 2** Temperature coefficient of surface tension and surface tension value at liquidus temperature for Si–Cu binary alloys

| | Liquidus temperature, K | Temperature coefficient, $10^{-4}$N/m K | Surface tension at liquidus temperature, N/m |
|---|---|---|---|
| $Si_{05}Cu_{95}$ | 1311 | −3.060 | 1.356 |
| $Si_{10}Cu_{90}$ | 1246 | −2.686 | 1.332 |
| $Si_{14.9}Cu_{85.1}$ | 1159 | −2.468 | 1.295 |
| $Si_{16}Cu_{84}$ | 1125 | −1.961 | 1.322 |
| $Si_{16.6}Cu_{85.4}$ | 1118 | −2.139 | 1.330 |
| $Si_{20}Cu_{80}$ | 1094 | −1.750 | 1.265 |
| $Si_{22.5}Cu_{77.5}$ | 1131 | −1.701 | 1.194 |
| $Si_{24}Cu_{76}$ | 1132 | −0.7399 | 1.151 |
| $Si_{25}Cu_{75}$ | 1131 | −0.1372 | 1.115 |
| $Si_{27.5}Cu_{72.5}$ | 1114 | −0.9351 | 1.100 |
| $Si_{30}Cu_{70}$ | 1075 | 0.02259 | 1.036 |
| $Si_{35}Cu_{65}$ | 1164 | 0.6864 | 0.974 |

the surface tension at the liquidus temperature. For the $Si_{35}Cu_{65}$ alloy, we obtained a positive temperature coefficient. For a pure metal, the temperature coefficient of surface tension has a negative value at all temperatures. On the other hand, in the case of alloys, the temperature coefficient of surface tension is not necessarily negative in all temperature regions. Some alloys have a positive temperature coefficient within a narrow temperature region. This phenomenon is related to entropic effects, reducing surface segregation [4]. Moreover, the previous results, using sessile drop method [9], also show positive temperature dependence, even over a wider composition range.

In order to discuss the composition dependence of surface tension, we calculate it using the ideal solution model and the Butler model. For calculation in the ideal solution model, we used the surface tension data of pure silicon [10] and copper [11], and, in the Butler model, we used experimental data of excess Gibbs energy reported by [12] additionally. Both models consider the effect of surface segregation due to the difference in surface tension between pure silicon and pure copper. In the ideal solution model, the surface concentrations of each component $C_{Si}^{surf}$ and $C_{Cu}^{surf}$ are given by

$$C_{Si}^{surf} = \frac{C_{Si}}{C_{Si} + C_{Cu}/\exp[A(\gamma_{Cu} - \gamma_{Si})/RT]}, \quad (8)$$

$$C_{Cu}^{surf} = \frac{C_{Cu}}{C_{Cu} + C_{Si}\exp[A(\gamma_{Cu} - \gamma_{Si})/RT]}. \quad (9)$$

where $\gamma_{Si}$ and $\gamma_{Cu}$ are the surface tension of pure silicon and copper, respectively, $R$ is the gas constant, and $T$ is the temperature of the alloy. $A$ is the averaged molar surface area [13], thus it is given by $A = 1.091V^{2/3}N_A^{1/3}$, where $V$ is the averaged molar volume, and $N_A$ is Avogadro's constant. Using the surface concentrations, the surface tension of the alloy given by the ideal solution model is:

$$\gamma = C_{Si}^{surf}\gamma_{Si} + C_{Cu}^{surf}\gamma_{Cu} = \frac{\gamma_{Si}C_{Si}}{C_{Si} + C_{Cu}\exp\left[-\frac{A(\gamma_{Cu}-\gamma_{Si})}{RT}\right]} + \frac{\gamma_{Cu}C_{Cu}}{C_{Cu} + C_{Si}\exp\left[\frac{A(\gamma_{Cu}-\gamma_{Si})}{RT}\right]} \quad (10)$$

Figure 7 shows that the experimental results do not agree well with either the ideal solution model or the Butler model. The Bulter model seems to at least reproduce the general trend correctly. We think that this difference is due to the effect of intermetallic compound clusters in the melt. In order to discuss this difference, we plotted the difference between the values of the ideal solution model and the experimental data in Fig. 8. In this figure, it can be seen that an extremum exists. This is the same result as obtained for the excess volume of this system. It demonstrates the effect of local fluctuations ascribable to intermetallic compound formation. However, in Fig. 8, the extremum appears at around 80–85 Cu-at%, i.e. on the copper-rich side of the intermetallic $\eta$ phase.

A model for systems forming intermetallic compounds was reported in Ref. [4]. This model is an extension of the ideal solution model. In this modified ideal solution model, the binding energy of clusters is taken into account for surface segregation factors. For this, the energy gain by surface segregation must include the energy to break a cluster of the form $SiCu_3$ on the surface. Therefore, Eqs. 8 and 9 are rewritten as,

$$C_{Si}^{surf,modified} = \frac{C_{Si}}{C_{Si} + C_{Cu}/\exp[(A(\gamma_{Cu} - \gamma_{Si}) - f(n+m)C_{Si}^{n}C_{Cu}^{m})/RT]}, \quad (11)$$

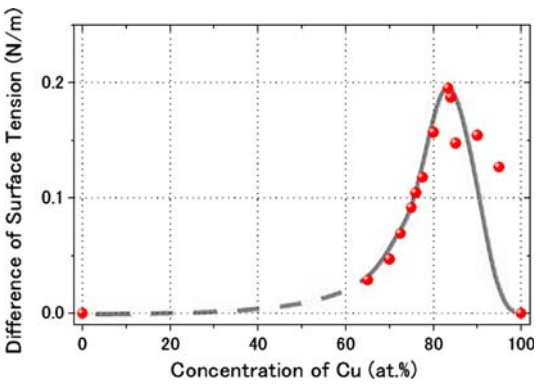


**Fig. 8** Composition dependence of the difference in surface tension between experimental and calculated data using the ideal solution model. A peak exists at 80–85 Cu at.%

$$C_{\mathrm{Cu}}^{\mathrm{surf,modified}} = \frac{C_{\mathrm{Cu}}}{C_{\mathrm{Cu}} + C_{\mathrm{Si}} \exp[(A(\gamma_{\mathrm{Cu}} - \gamma_{\mathrm{Si}}) - f(n+m)C_{\mathrm{Si}}^{n} C_{\mathrm{Cu}}^{m})/RT]}, \quad (12)$$

where, $f$ is the molar binding energy of the cluster and $n$ and $m$ are the ratio of the number of atoms of the cluster. Thus, in this case, $n = 1$ and $m = 3$. Figure 9 shows the calculation result of this modified ideal solution model. The value of the molar binding factor $f$ was obtained as a fit parameter. The value of $f/RT$ was 4.258. This model could fit better than both the normal ideal solution model and the Butler model in this Si–Cu binary alloy system.

As discussed previously, using this modified ideal solution model, the surface tension of the Si–Cu binary alloy system is more accurately expressed. However, the difference between this modified ideal solution model and the normal ideal solution model has a peak at Cu-75 at.%, while the difference between our experimental data and the normal ideal solution model has a peak at Cu-80–85 at.%.

In the modified ideal solution model, the energy to break a cluster of the intermetallic compound on the surface is included in the energy gain by surface segregation. Therefore, we thought it is better to use the value of the atomic concentration of the surface rather than the atomic concentration of the bulk in terms of energy to break a cluster. Consequently, we rewrite Eqs. 11 and 12

$$C_{\mathrm{Si}}^{\mathrm{surf,modified}} = \frac{C_{\mathrm{Si}}}{C_{\mathrm{Si}} + C_{\mathrm{Cu}} / \exp\left[(A(\gamma_{\mathrm{Cu}} - \gamma_{\mathrm{Si}}) - f(n+m)C_{\mathrm{Si}}^{\mathrm{surf}^{n}} C_{\mathrm{Cu}}^{\mathrm{surf}^{m}})/RT\right]}, \quad (13)$$

$$C_{\mathrm{Cu}}^{\mathrm{surf,modified}} = \frac{C_{\mathrm{Cu}}}{C_{\mathrm{Cu}} + C_{\mathrm{Si}} \exp[(A(\gamma_{\mathrm{Cu}} - \gamma_{\mathrm{Si}}) - f(n+m)C_{\mathrm{Si}}^{\mathrm{surf}^{n}} C_{\mathrm{Cu}}^{\mathrm{surf}^{m}})/RT]}. \quad (14)$$

Figure 9 shows the result of this calculation using the surface atomic concentration. In this fitting, the same value $f$ given above is used. The result is in good agreement with our experimental data.

Using Eqs. 13 and 14, we obtained the surface segregation rate of this Si–Cu binary system. Figure 10 shows the surface coverage of Cu against the Cu concentration of bulk. It shows that in the region over 90% of Cu, the coverage changes little; in the region between 80 and 85%, however, the coverage changes drastically. This means that the Si–Cu binary system avoids the surface segregation of the composition $Si_{25}Cu_{75}$. Figure 11 shows the deviation of surface coverage of Cu with respect to the bulk concentration of Cu as a function of the surface concentration of Cu. The curve shows a maximum around 75 at.% of Cu. This also suggests that the Si–Cu binary system avoids the surface segregation of the composition $Si_{25}Cu_{75}$. As

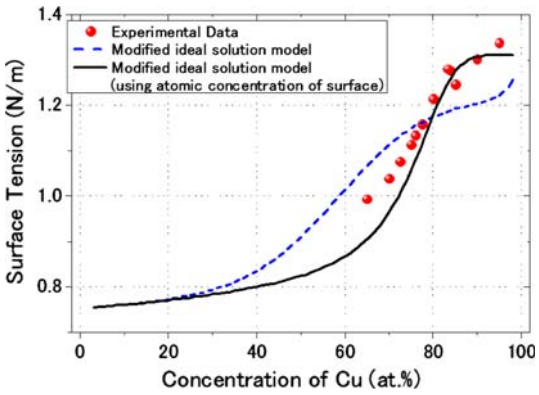


**Fig. 9** Experimental data and calculated results using the modified ideal solution model. The *dashed line* was obtained using Eqs. 11 and 12, and the *solid line* was obtained using Eqs. 13 and 14

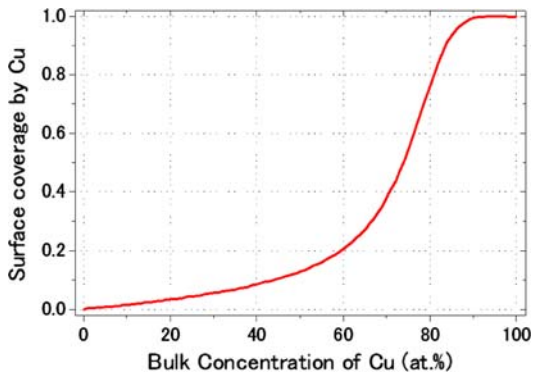


**Fig. 10** Surface coverage of Cu versus Cu bulk concentration

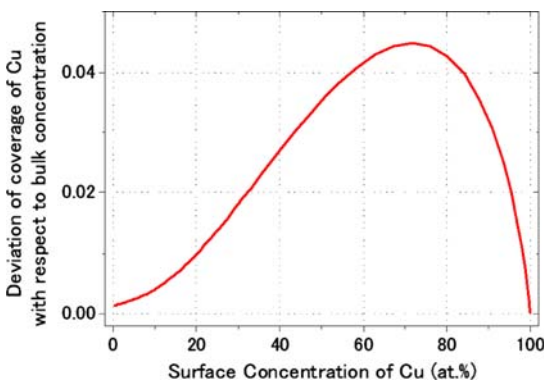


**Fig. 11** The deviation of Cu surface coverage with respect to bulk concentration as a function of the surface concentration of Cu

discussed above, the bulk composition does not equal the surface composition.

## Summary

We accurately measured the density and surface tension of Si–Cu binary system using an electromagnetic levitation method that has advantages in measuring thermophysical properties over a wide temperature range. The composition dependence of the excess volume shows a minimum at the intermetallic compound composition $SiCu_3$. Moreover, the composition dependence of the 'excess' surface tension, i.e. the difference in surface tension from an ideal solution model, shows a peak slightly at the Cu-rich side of the intermetallic compound composition. We attribute both peaks to the existence of (metastable) clusters of intermetallic composition in the liquid. In the latter case, the effect is the largest when the surface composition corresponds to the intermetallic compound composition. Therefore, the peak is slightly shifted to the Cu-rich side.

**Acknowledgements** One of the authors (M.A.) gratefully appreciates the financial support from Fujukai Foundation, and a part of this study was supported by SENTAN, JST; support was also provided by a Grant-in-Aid for Scientific Research (KAKENHI No. 19560747).

## References

1. ASM International binary alloy phase diagrams (The Materials Information Society) CD-ROM, Second edn. ASM International Materials Park, Ohio (1996)
2. Butler J (1935) Proc R Soc A135:348
3. Tanaka T (1999) MRS Bull 24:45
4. Egry I (2005) Int J Thermophys 26:931
5. Brillo J et al (2003) Int J Thermophys 24:1155
6. Egry I et al (2005) Meas Sci Tech 16:426
7. Cummings DL, Blackburn DA (1991) J Fluid Mech 224:395
8. Watanabe M et al (2007) Faraday Discuss 136:279
9. Khilya GP, Ivashchenko Y (1973) Dopov Akad Nauk Ukr RSR B 35:69 (reported by Keene BJ et al (1987) in Surf Interface Anal 10:367)
10. Fujii H et al (2006) Acta Materialia 54:1221
11. Mills KC (2001) Recommended values of thermophysical properties for selected commercial alloys. Asm Intl, Cambridge
12. Miki T et al (2002) ISIJ Int 42:1071
13. Turkdogan T (1980) Physical chemistry of high temperature technology. Academic Press, New York